ISIJ International, Vol. 50 (2010), No. 8, pp. 1078–1083

Carbide Capacity of $CaO–SiO_2–MnO$ Slag for the Production of Manganese Alloys

Joo Hyun PARK,[1)] Geun Ho PARK[1)] and Young E. LEE[2)]

1) School of Materials Science and Engineering, University of Ulsan, Ulsan 680-749 Korea. E-mail: basicity@mail.ulsan.ac.kr
2) Metallic Materials Research Institute, Dongbu Metal Co., Ltd., Donghae 240-143 Korea.

(*Received on March 10, 2010; accepted on May 27, 2010*)

The carbide capacity of the $CaO–SiO_2–MnO$ slag, which is the main system produced during Mn alloys processes, through the wide composition region has been measured at 1 773 K to understand the effective slag composition on the solubility of carbon in molten slags during SiMn production processes. The carbide capacity is strongly affected by slag composition and this tendency can be reasonably estimated by employing the activity of lime and the activity coefficient of CaC_2 as a thermodynamic factors affecting carbide capacity. Considering the high concentration of MnO during SiMn smelting process, the lime to silica ratio of 0.8 ($\pm$0.1) is recommended in view of high ability of carbon dissolution. The carbide capacity of the $CaO–SiO_2–MnO$ slag can be expressed as a linear function of the activity of lime and the optical basicity. The carbide capacity of the $CaO–SiO_2–MnO$ slag increases more significantly than the sulfide capacity does as the basicity of the slag increases.

KEY WORDS: carbide capacity; carbon solubility; SiMn production; activity; activity coefficient; basicity; stability.

1. Introduction

Manganese rich slag is generated from the high carbon ferromanganese (HC FeMn) production process. This slag generally contains 30 to 40 mass% MnO.[1,2)] In addition to its high manganese content, it also has the advantage of high Mn/Fe ratio, low phosphorus content, low fine content and low cost.[3)] The possibility of using such a slag for the production of silicomanganese (SiMn) alloys seems to be very attractive and has a strong economic impact on the production process. There has been a shift in demand away from the use of HC FeMn towards SiMn and refined alloys of both.

Low carbon SiMn with 20 to 30 mass% Si is produced by upgrading standard SiMn alloy by the addition of Si wastes from ferrosilicon industry. The Mn(–Fe)–Si–C system is very important in production of SiMn.[1)] Graphite is the stable phase in the lower Si range, whereas silicon carbide (SiC) becomes the stable phase at higher Si content, *e.g.* 22 mass% Si when [C]=1.0 mass% at 1 773 K.[4)] Therefore, the addition of Si decreases the solubility limit of carbon in SiMn alloy melt, resulting in a nucleation and growth of SiC particles in the melt. The carbide particles are believed to float up and partly dissolve into the slags at slag/metal interface. Notwithstanding the well-known thermodynamics of the metallic systems, there are few experimental data for understanding the slag refining mechanism of carbon (or SiC) from SiMn melt.

There are several studies for the measurement of carbon solubility of metallurgical slags as carbide (C_2^{2-}) or carbonate (CO_3^{2-}) according to oxygen partial pressure.[5–10)] Based on the previous works, one can conclude that the stable ionic form is carbide under reducing conditions that is in correspondence to the manganese alloys production. The solubility of carbide and thus carbide capacity defined in Eqs. (1) and (2) generally increases with increasing basicity in the lime-based silicate, aluminate, and aluminosilicate melts with and without fluorspar,[6,8,10–14)] whilst there are some experimental results for an increase in the carbon solubility as the content of acidic oxides (SiO_2 and B_2O_3) increases.[8,10,15,16)]

$$2C(s) + O^{2-}(slag) = C_2^{2-}(slag) + \frac{1}{2}O_2(g) \quad \text{.....(1)}$$

$$C_{C_2^{2-}} \equiv \frac{K_{(1)} \cdot a_{O^{2-}}}{f_{C_2^{2-}}} = \frac{(\text{mass\% } C_2^{2-}) \cdot p_{O_2}^{1/2}}{a_C^2} \quad \text{.....(2)}$$

where $K_{(1)}$, a_i, $f_{C_2^{2-}}$, and p_{O_2} are, respectively, the equilibrium constant of Eq. (1), the activity of i, the activity coefficient of carbide ions, and the oxygen partial pressure. Hence, the carbide capacity is a function of basicity and the stability of carbide ions in molten slags at a fixed temperature.

Even though there are some experimental results for the solubility of carbon in the lime-based slags,[5–16)] the carbide capacity of the MnO-containing slag is hardly found. The only system containing MnO in view of carbon solubility is the BaO–MnO flux, where the carbon solubility increased with increasing content of BaO not only due to a basic characteristic of BaO but also due to a strong ionic attrac-

tion between Ba^{2+} cation and carbide anion.[18] Therefore, in the present study, the carbide capacity of the CaO–SiO_2–MnO slag, which is the main system produced during Mn alloys processes, through the wide composition region has been measured at 1 773 K to understand the effective slag composition on the solubility of carbon in molten slags during SiMn production processes.

2. Experimental

A super-kanthal electric resistance furnace was used for an equilibration of the CaO–SiO_2–MnO slag and gas phase at 1 773 K. The temperature was controlled within ±2 K using an R-type (Pt–13%Rh/Pt) thermocouple and a proportional integral differential controller. The furnace temperature was also calibrated using a B-type (Pt–30%Rh/Pt–6%Rh) thermocouple. The slag samples were prepared using reagent-grade SiO_2, MnO and CaO calcined from $CaCO_3$ at 1 273 K. For the saturation conditions with silica and dicalcium silicate phase, a piece of pure quartz and lime crystals (>99.9 mass%) are located in the slag. A schematic diagram of the experimental apparatus is shown elsewhere.[8,9]

The slag sample of 4 g was maintained in a graphite crucible under CO atmosphere (200 mL/min) to control the oxygen partial pressure by C/CO equilibrium reaction, as given in Eq. (3).[19]

$$\mathrm{C(s)} + \frac{1}{2}\mathrm{O_2(g)} = \mathrm{CO(g)},$$
$$\Delta G^\circ = -114\,000 - 85.8T \quad \mathrm{(J/mol)} \quad \text{.....(3)}$$

The impurities such as CO_2 and H_2O in the CO gas were removed by passing through silica gel, drierite®, magnesium perchlorate, and soda lime. The equilibration time was predetermined to be 15 h. After equilibrating, the sample was quickly drawn from the furnace and quenched by Ar flushing and water. The quenched samples were crushed to less than 100 μm using stainless and agate mortars for chemical analysis. The content of total carbon and each component in the slags were determined by a combustion analyzer (LECO, CS-200) and X-ray fluorescence spectroscopy (Bruker, S4 Explorer). The equilibrium composition and carbide capacity of the slags measured in this study are shown in **Table 1**.

3. Results and Discussion

3.1. Effect of Slag Composition on Carbide Capacity of CaO–SiO_2–MnO Slag

The carbide capacity of the silica saturated ternary system at 1 773 K is shown as a function of MnO content in **Fig. 1**. The capacity decreases with increasing content of MnO up to about 35 mass%, followed by nearly constant value with some scatters. As introduced previously in Eqs. (1) and (2), the carbide capacity is a function of basicity and the stability of carbide ions in the slags. In this study, because of the thermodynamic constraint, it is assumed that the activity of O^{2-} ions, $a_{O_2^-}$ is directly proportional to that of lime, a_{CaO} based on Eq. (4).

Table 1. Experimental composition (mass%) and the carbide capacity of the CaO–SiO_2–MnO slag at 1 773 K.

CaO	SiO_2	MnO	log $C_{carbide}$
0.0	51.3	50.8	-9.69
3.1	51.2	45.6	-9.64
5.5	52.1	43.2	-9.61
10.1	54.4	34.4	-9.75
15.7	58.1	26.2	-9.58
21.5	51.8	25.9	-9.48
20.2	57.9	21.9	-9.72
26.3	49.8	22.1	-9.38
30.1	42.8	24.6	-9.29
22.0	59.1	17.6	-9.51
27.2	53.8	18.1	-9.53
30.7	50.9	17.4	-9.24
35.6	46.0	17.2	-9.08
40.5	42.1	16.7	-9.30
30.1	58.3	10.4	-9.59
42.1	43.9	14.1	-9.42
42.8	44.0	13.0	-9.38
49.4	44.3	6.9	-9.50
53.6	41.5	4.4	-8.71
60.0	42.1	0.0	-8.92
50.9	47.4	0.0	-9.31
41.0	56.9	0.0	-9.48
35.8	64.2	0.0	-9.43

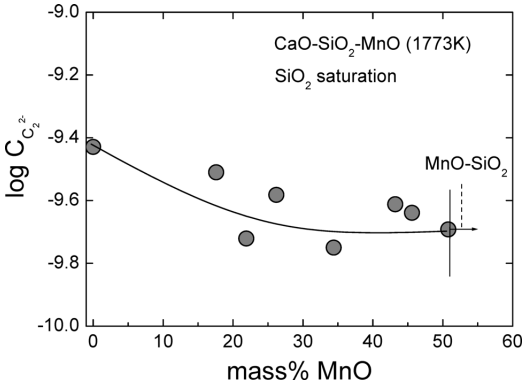

Fig. 1. Dependence of the carbide capacity of the silica saturated CaO–SiO_2–MnO slag system on the content of MnO at 1 773 K.

$$(\mathrm{CaO}) = (\mathrm{Ca^{2+}}) + (\mathrm{O^{2-}}) \quad \text{.....(4)}$$

Furthermore, the activity coefficient of carbide ions in the slags can be estimated by employing the activity coefficient of CaC_2, which is the most stable molecular species in the present system. The formation reaction of CaC_2 and thus the activity coefficient of CaC_2 are given in Eqs. (5) and (7), respectively.[19–21]

$$\mathrm{CaO(s)} + 2\mathrm{C(s)} = \mathrm{CaC_2(s)} + \frac{1}{2}\mathrm{O_2(g)},$$
$$\Delta G^\circ = 568\,000 - 144T \quad \mathrm{(J/mol)} \quad \text{.....(5)}$$

$$K_{(5)} = \frac{\gamma_{CaC_2} \cdot X_{CaC_2} \cdot p_{O_2}^{1/2}}{a_{CaO} \cdot a_C^2} \quad \text{.....(6)}$$

$$\log \gamma_{CaC_2} = \log a_{CaO} - \log X_{CaC_2} - \frac{1}{2}\log p_{O_2} + \log K_{(5)} \quad ...(7)$$

where the activity of carbon is unity because graphite crucible was used in the experiments. The calculated value of the activity of CaC_2 is less than about 10^{-4} under present experimental conditions. Therefore, a discussion in this study will be limited to the dissolved carbide ions in molten slags. In this study, the activity of lime was calculated using commercial thermochemical computing software, FactSage™6.1 with *FToxid* database.[22] In this database, the systems containing MnO with major components such as CaO and SiO_2, that is CaO–MnO, MnO–SiO_2, and CaO–SiO_2–MnO, are fully evaluated and optimized based on Gibbs free energy minimization principle.[23–25] The thermodynamic description for the CaO–MnO–SiO_2 system reproduces all available and reliable experimental data such as phase diagrams and activity in the molten slag, as well as slag–metal (liquid iron and liquid manganese alloys) equilibria within experimental error range.[23] This description is consistent with thermodynamic description of sub-binary systems, and also has been successfully extrapolated to higher order system containing Al_2O_3.[24] Although there is no experimental data for activity of CaO to be directly compared with the model calculations, it is believed that the calculated activity of CaO from the thermodynamic database should be close to reality.

The calculated activity of lime and the activity coefficient of CaC_2 in silica saturated slag system are shown in **Fig. 2**. The activity of lime, $\log a_{CaO}$ linearly decreases with increasing content of MnO up to about 35 mass%, whereas the activity coefficient of CaC_2, $\log \gamma_{CaC_2}$ is independent of MnO content. However, both of thermodynamic indicators commonly decrease at MnO>35 mass%, resulting in a constant carbide capacity in the highly acidic slag such as silica saturation condition as shown in Fig. 1.

The carbide capacity of the CaO–SiO_2–MnO system (mass% MnO/mass% SiO_2=0.3 to 0.4) at 1 773 K is shown as a function of lime content in **Fig. 3**. The capacity exhibits a maximum value at about 35 mass% CaO and the lowest at silica saturation composition. The dependence of the activity of lime and the activity coefficient of CaC_2 on the lime content is calculated and is shown in **Fig. 4**. The activity of lime linearly increases in nature as its concentration increases, while the activity coefficient of CaC_2 does not change to 35 mass% CaO, followed by an abrupt increase by increasing the content of lime. Thus, it is proposed that highly basic composition is not recommended in view of carbon absorption in the CaO–SiO_2–MnO slag of which MnO/SiO_2=0.3 to 0.4, close to the SiMn tapping slag, probably due to a decrease in the stability of carbide ions.

The effect of silica content on the carbide capacity of the slag system of which CaO/MnO=1 is shown in **Fig. 5**, where the capacity is linearly decreases with increasing content of silica. This mainly originates from a strong de-

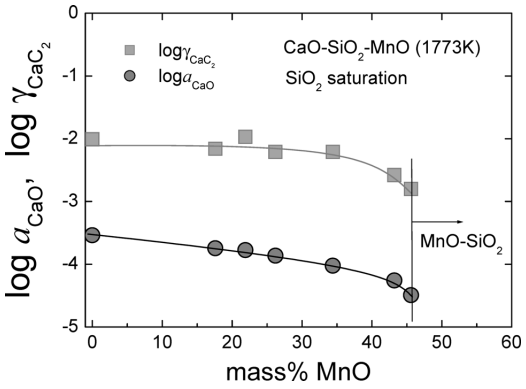

Fig. 2. Calculated activity of lime and activity coefficient of CaC_2 in the silica saturated CaO–SiO_2–MnO slag system as a function of the content of MnO at 1 773 K.

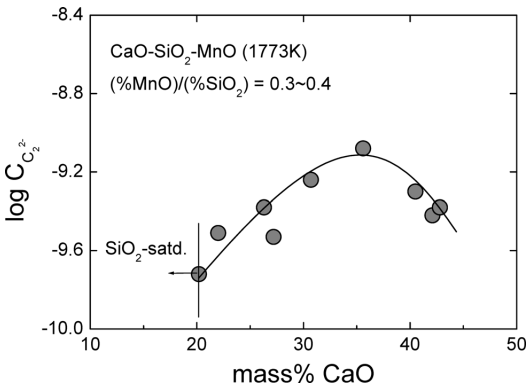

Fig. 3. Dependence of the carbide capacity of the CaO–SiO_2–MnO (MnO/SiO_2=0.3–0.4) system on the content of lime at 1 773 K.

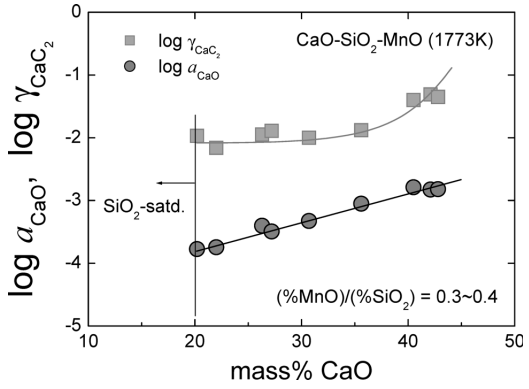

Fig. 4. Calculated activity of lime and activity coefficient of CaC_2 in the CaO–SiO_2–MnO (MnO/SiO_2=0.3–0.4) system as a function of lime content at 1 773 K.

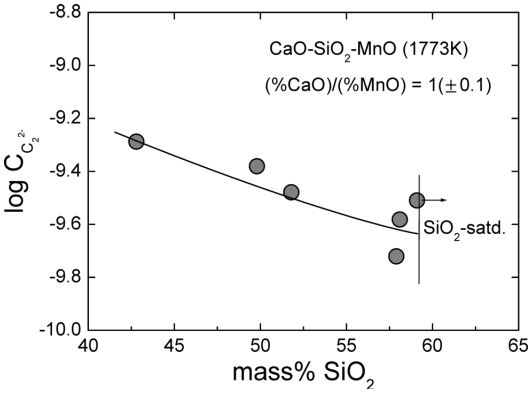

Fig. 5. Dependence of the carbide capacity of the CaO–SiO_2–MnO (CaO/MnO=1) system on the content of silica at 1 773 K.

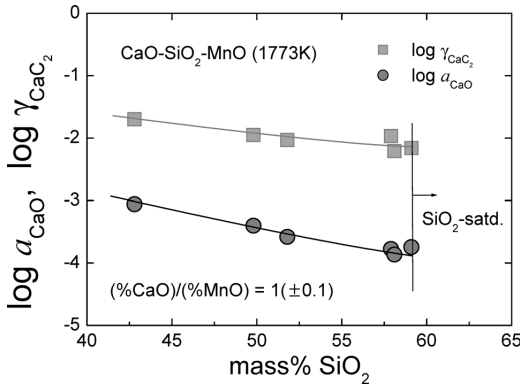

Fig. 6. Calculated activity of lime and activity coefficient of CaC_2 in the CaO–SiO_2–MnO (CaO/MnO=1) system as a function of silica content at 1 773 K.

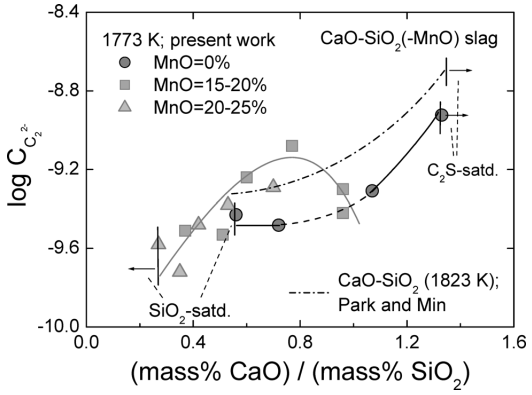

Fig. 7. Dependence of the carbide capacity of the CaO–SiO_2–MnO slag on the ratio of CaO to SiO_2 at 1 773 K.

creasing tendency of the activity of lime, whereas a slight decrease in the activity coefficient of CaC_2 is estimated as the content of silica increases as shown in **Fig. 6**.

The effect of lime to silica ratio (C/S ratio) on the carbide capacity is shown in **Fig. 7** according to the level of MnO content. For comparison, the experimental data for the CaO–SiO_2 binary system measured at 1 823 K is also shown.[13] In the CaO–SiO_2 binary system, the carbide capacity continuously increases with increasing C/S ratio in nature based on Eqs. (1) and (2). It is interesting that the capacity also increases as temperature increases, indicating that the experimental data in the present work is principally acceptable. However, in the CaO–SiO_2–MnO ternary slag, the carbide capacity shows a maximum value at about C/S=0.8 and the content of MnO from 15 to 25 mass% does not affect the carbide capacity. Hence, it is suggested that the addition of MnO from 10 to 30 mass% at high temperatures can enhance the absorption of carbon in HCFeMn and MCSiMn slags. The effect of C/S ratio on the activity of lime and the activity coefficient of CaC_2 is calculated and is shown in **Fig. 8**. The activity of lime continuously increases with increasing value of C/S in nature. Here, the effect of MnO on the $\log a_{CaO}$ is not significant. The activity coefficient of CaC_2 in the CaO–SiO_2 binary system increases by increasing the value of C/S, while it decreases at highly basic composition such as Ca_2SiO_4 saturation condition. However, the activity coefficient of CaC_2 in the CaO–SiO_2–MnO ternary system linearly increases as C/S ratio increases irrespective of MnO content, followed by an abrupt increase in the $\log \gamma_{CaC_2}$.

Therefore, it is qualitatively concluded that the stability of carbide increases in highly basic composition in the CaO–SiO_2 binary system, whereas it decreases in the relatively basic (C/S>0.8) ternary slag system probably due to a competitive interaction between MnO and CaO. However, the more detailed research is required; for example, a structural behavior of Ca^{2+} and Mn^{2+} cations in silicate melts. The iso-carbide capacity lines of the CaO–SiO_2–MnO slag at 1 773 K is schematically represented in **Fig. 9**. Here, the phase diagram was calculated using FactSage™6.1. The composition of FeMn and SiMn tapping slag is also represented as 'A' and 'B', respectively.[1] Consequently, the optimum compositional window in view of carbon absorption capability during Mn alloys production is located between

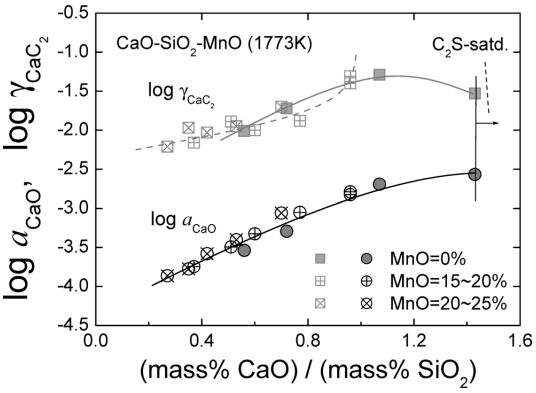

Fig. 8. Calculated activity of lime and activity coefficient of CaC_2 in the CaO–SiO_2–MnO slag as a function of CaO/SiO_2 ratio at 1 773 K.

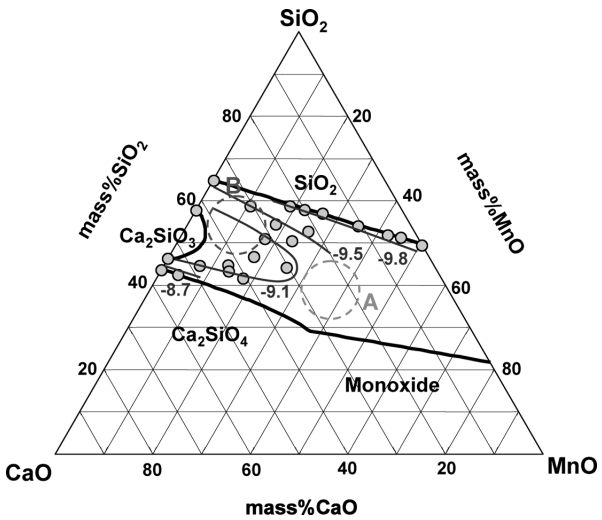

Fig. 9. Iso-carbide capacity lines in the CaO–SiO_2–MnO slag at 1 773 K. Numerical values represent the $\log C_{C_2^{2-}}$. A; HCFeMn slag. B; SiMn slag.

FeMn and SiMn slag that currently operated.

3.2. Relationship between Carbide Capacity and Refining Indices of CaO–SiO_2–MnO Slag

The carbide capacity of the CaO–SiO_2–MnO ternary system (MnO>10 mass%) at 1 773 K is plotted against the activity of lime in **Fig. 10**. The capacity, $\log C_{C_2^{2-}}$ is constant at

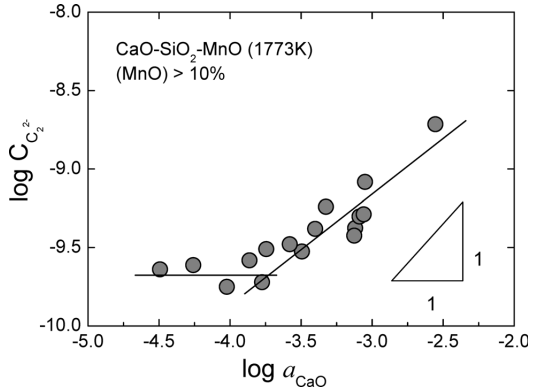

Fig. 10. Relationship between the carbide capacity and the activity of lime in the $CaO–SiO_2–MnO$ slag at 1 773 K.

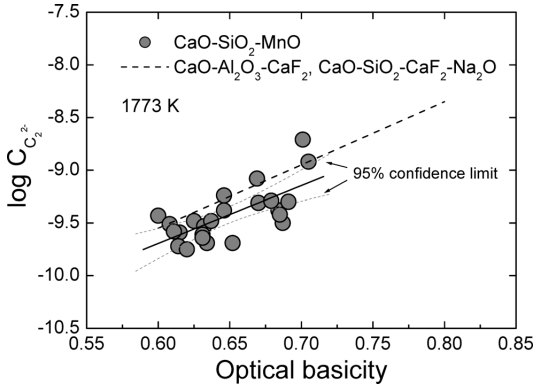

Fig. 11. Relationship between the carbide capacity and the optical basicity of the $CaO–SiO_2–MnO$ slag at 1 773 K.

$a_{CaO}<10^{-3.8}$, which corresponds to the nearly silica saturation condition, while it linearly increases by increasing the value of $\log a_{CaO}$ with a slope of 0.75 in liquid slag area. This is slightly lower than an expected value of unity on the assumption that there is a direct proportionality between $a_{O^{2-}}$ and a_{CaO} as well as a negligible compositional dependency of $f_{C_2^{2-}}$ in Eq. (2). Therefore, one can expect that the stability of carbide is affected by slag composition and this tendency is significant in the strongly acidic composition.

Figure 11 exhibits the relationship between the carbide capacity and the optical basicity of the slag at 1 773 K. Here, the optical basicity of molten slags (Λ) was calculated from Eq. (8).[26,27]

$$\Lambda = \frac{\sum x_i n_i \Lambda_i}{\sum x_i n_i} \quad \text{.....(8)}$$

where x_i, n_i and Λ_i are, respectively, the mole fraction, the number of oxygen in each oxide, and the theoretical optical basicity of component i. The theoretical optical basicity of CaO, SiO_2 and MnO was taken to be 1.0, 0.48 and 1.0, respectively, which was originally suggested.[26,27] Actually, Sosinsky and Sommerville proposed an empirical optical basicity of MnO to be 1.2 in view of sulfide capacity approximation.[28] This empirical value ($\Lambda_{MnO}=1.2$) could be applicable in case of sulfide capacity only, because the MnO is a strong sulfide former. The carbide capacity of the $CaO–SiO_2–MnO$ slag shows a good linear correspondence with the optical basicity within some experimental scatters with a 95% confidence limit. Also, the relationship between carbide capacity, $\log C_{C_2^{2-}}$ and optical basicity in the $CaO–SiO_2–MnO$ slag is reasonably close to that of $CaO–Al_2O_3–CaF_2$ and $CaO–SiO_2–CaF_2–Na_2O$ slags.[14,15]

It is meaningful to discuss the relationship between carbide and sulfide capacities of the slag in view of the basicity difference and the relative stability of each reaction product.[29] A relationship between sulfide capacity and carbide capacity of various slags is shown in **Fig. 12**. From a definition of sulfide capacity (Eq. (10)), the correlation between them is deduced as shown in Eq. (11).

$$\frac{1}{2}S_2(g) + O^{2-}(\text{slag}) = S^{2-}(\text{slag}) + \frac{1}{2}O_2(g) \quad \text{.....(9)}$$

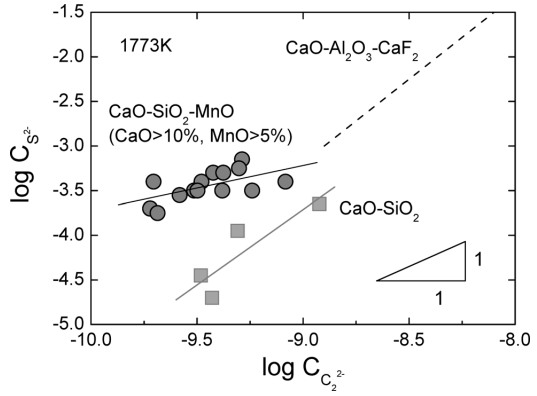

Fig. 12. Relationship between the carbide capacity and the sulfide capacity of the $CaO–SiO_2–MnO$ slag at 1 773 K.

$$C_{S^{2-}} \equiv \frac{K_{(9)} \cdot a_{O^{2-}}}{f_{S^{2-}}} = (\text{mass\% } S^{2-}) \cdot \left(\frac{p_{O_2}}{p_{S_2}}\right)^{1/2} \quad \text{.....(10)}$$

$$\log C_{S^{2-}} = \log C_{C_2^{2-}} + \log \frac{f_{C_2^{2-}}}{f_{S^{2-}}} + \log \frac{K_{(9)}}{K_{(1)}} \quad \text{.....(11)}$$

Although a good linearity is observed between them, the slope of the line is estimated to be about 0.53 in the $CaO–SiO_2–MnO$ slag, whereas it is 1.6 and 1.8 in the $CaO–SiO_2$ and $CaO–Al_2O_3–CaF_2$ slags, respectively.[13,14] This indicates that the sulfide capacity is more pronounced than the carbide capacity as the basicity increases in the $CaO–SiO_2$ and $CaO–Al_2O_3–CaF_2$ slags. However, the carbide capacity increases more drastically than the sulfide capacity does under the same degree of basicity increase in the $CaO–SiO_2–MnO$ slag. Thus, the ratio $f_{C_2^{2-}}/f_{S^{2-}}$ in Eq. (11) would not be constant but strongly affected by slag composition.

4. Conclusions

The carbide capacity of the $CaO–SiO_2–MnO$ slag, which is the main system produced during Mn alloys processes, through the wide composition region has been measured at 1 773 K to understand the effective slag composition on the solubility of carbon in molten slags during SiMn production processes. The conclusions in the present study are

summarized as follows.

(1) The carbide capacity is strongly affected by slag composition and this tendency can be reasonably estimated by employing the activity of lime and the activity coefficient of CaC_2 as a thermodynamic factors affecting carbide capacity.

(2) Considering the high concentration of MnO during SiMn smelting process, the lime to silica ratio of 0.8 ($\pm$0.1) is recommended in view of high ability of carbon dissolution.

(3) The carbide capacity of the CaO–SiO_2–MnO (MnO$>$10 mass%) system can be expressed as a linear function of the activity of lime and the optical basicity.

(4) The carbide capacity of the CaO–SiO_2–MnO slag increases more significantly than the sulfide capacity does as the basicity of the slag increases. However, the structural role of Ca^{2+} and Mn^{2+} in silicate melts should be further investigated in order to fully understand the effect of basicity and the stability of the reaction products on the capacity of molten slags.

Acknowledgement

The authors are grateful to Prof. Y. B. Kang, Graduate Institute of Ferrous Technology, POSTECH, Korea, for his fruitful comment on the validity of FactSage™ databases.

REFERENCES

1) S. E. Olsen, M. Tangstad and T. Lindstad: Production of Manganese Ferroalloys, SINTEF and Tapir Academic Press, Trondheim, Norway, (2007), 43.
2) E. C. Vanderstaay, D. R. Swinbourne and M. Monteiro: *Min. Proc. Extr. Metall. (Trans. Inst. Min. Metall. C)*, **113** (2004), 38.
3) A. Ahmed, A. El-Mohammady, M. Eissa and K. El-Fawakhry: *Steel Res. Int.*, **78** (2007), 24.
4) K. Tang and S. E. Olsen: *Metall. Mater. Trans. B*, **37B** (2006), 599.
5) N. Sano, W. K. Lu, P. V. Riboud and M. Maeda: Advanced Physical Chemistry for Process Metallurgy, Academic Press, San Diego, CA, (1997), 45.
6) M. Kuwata and H. Suito: *Metall. Mater. Trans. B*, **27B** (1996), 57.
7) M. Mori, K. Morita and N. Sano: *Metall. Mater. Trans. B*, **28B** (1997), 1257.
8) J. H. Park and D. J. Min: *Metall. Mater. Trans. B*, **30B** (1999), 1045.
9) I. Sohn, D. J. Min and J. H. Park: *Steel Res.*, **70** (1999), 215.
10) I. H. Jung: *ISIJ Int.*, **46** (2006), 1577.
11) K. Schwerdtfeger and H. G. Schubert: *Metall. Trans. B*, **8B** (1977), 535.
12) R. A. Berryman and I. D. Sommerville: *Metall. Trans. B*, **23B** (1992), 223.
13) J. H. Park and D. J. Min: *ISIJ Int.*, **40** (2000), S96.
14) J. H. Park, D. J. Min and H. S. Song: *ISIJ Int.*, **42** (2002), 127.
15) J. H. Park and D. J. Min: *ISIJ Int.*, **44** (2004), 223.
16) J. H. Swisher: *Trans. AIME*, **242** (1968), 2033.
17) K. R. Lee and H. Suito: *Steel Res.*, **67** (1996), 87.
18) Y. Watanabe, K. Kitamura, I. P. Rachev, F. Tsukihashi and N. Sano: *Metall. Trans. B*, **24B** (1993), 339.
19) E. T. Turkdogan: Physical Chemistry of High Temperature Technology, Academic Press, New York, (1980), 1.
20) T. Wakasugi and N. Sano: *Metall. Trans. B*, **20B** (1989), 431.
21) H. Ono, A. Kobayashi, F. Tsukihashi and N. Sano: *Metall. Trans. B*, **23B** (1992), 313.
22) www.factsage.com
23) Y. B. Kang, I. H. Jung, S. A. Decterov, A. D. Pelton and H. G. Lee: *ISIJ Int.*, **44** (2004), 965.
24) Y. B. Kang, I. H. Jung, S. A. Decterov, A. D. Pelton and H. G. Lee: *ISIJ Int.*, **44** (2004), 975.
25) C. Bale, E. Belisle, P. Chartrand, S. A. Decterov, G. Eriksson, K. Hack, I. H. Jung, Y. B. Kang, J. Melancon, A. D. Pelton, C. Robelin and S. Petersen: *Calphad*, **33** (2009), 295.
26) J. A. Duffy: *J. Non-Cryst. Solids*, **109** (1989), 35.
27) J. A. Duffy: *J. Chem. Educ.*, **73** (1996), 1138.
28) D. J. Sosinsky and I. D. Sommerville: *Metall. Trans. B*, **17B** (1986), 331.
29) C. Wagner: *Metall. Trans. B*, **6B** (1975), 405.